Pergamon

Cement and Concrete Research, Vol. 25, No. 5, pp. 1011-1022, 1995

0008-8846/95 $9.50+.00

0008-8846(95)00096-8

MODELING OF ELECTROMAGNETIC WAVE SCATTERING BY CONCRETE SPECIMENS

Oral Büyüköztürk and Hong C. Rhim
Department of Civil and Environmental Engineering
Massachusetts Institute of Technology
Cambridge, MA. 02139, U.S.A.

(Refereed)
(Received August 22, 1994)

ABSTRACT

This paper presents a novel application of finite difference-time domain (FD-TD) modeling to concrete to study the interaction of concrete with electromagnetic waves. The purpose of this work is to visualize the propagation of the electromagnetic fields in a dielectric medium of concrete in an effort to obtain one-dimensional images of a concrete target for nondestructive testing purposes. A Gaussian pulse plane wave is directed to laboratory size concrete specimens as an excitation source. Snap shots of computer simulation are shown to display wave propagation and scattering through and by the concrete specimens. Geometry of the targets is varied with different dimensions, and with or without an inclusion.

Introduction

The radar method is becoming one of the major nondestructive testing (NDT) techniques for concrete structures (1) as the need for the use of NDT techniques is increasing. The radar method has generally been used for NDT of pavements and bridge decks for civil engineering applications (2, 3). Recently, an attempt has been made to expand the capability of the radar method for NDT of structural elements of concrete structures (4). The use of electromagnetic wave scattering to image the interior configurations of concrete structures is a powerful tool for nondestructive remote sensing. The method involves the study of electromagnetic wave interaction with various concrete targets and a numerical technique which can simulate wave scattering by a dielectric medium such as concrete to examine numerous electromagnetic phenomena on a computer. Interpretation of echo grams from radar measurements for NDT of concrete structures hinges on an understanding of how electromagnetic waves propagate in concrete. In that respect, the study of forward modeling with known material and geometric parameters of concrete can provide valuable information as to how the wave propagates through and scatters by a concrete target. A candidate numerical modeling approach for this purpose is the finite difference-time domain (FD-TD) solution of Maxwell's curl equations, which are the governing equations of the electromagnetic fields (5, 6). The FD-TD is a marching-in-time procedure which can simulate continuous wave propagation in concrete. The technique is flexible in simulating objects with different geometry and wave sources. The method is especially suited for visualizing the electromagnetic phenomena, since electric and magnetic fields are calculated everywhere within a computational domain as a function of time (7).

This paper presents an application of the FD-TD numerical modeling technique to selected laboratory size concrete specimens. Electromagnetic wave scattering phenomena by three different types of concrete specimens using the FD-TD method are presented. One-dimensional images of the specimens, which represent the interior configurations of the targets, are obtained from the numerical study. The outside dimensions of the specimens are varied to examine the effect of target sizes on the wave propagation and scattering. The specimens are modeled with or without an inclusion to study the detectability of the inclusion. The issues involved in the use of the FD-TD method on concrete specimens for NDT purposes are also discussed.

Modeling Using the Finite Difference-Time Domain (FD-TD) Method

The FD-TD technique involves approximating Maxwell's equations in a differential form by center differences in space and time (7). The location at which electric and magnetic fields are calculated are positioned on a grid for two-dimensional problems. Boundary conditions are enforced at the outer boundary of the computational domain and at all dielectric and conducting interfaces. At the outer boundary, a second-order absorbing boundary condition is utilized in order to simulate unbounded space beyond the computational domain (8).

The incident wave used for the modeling is a Gaussian pulse plane wave, $V(t) = e^{-2(t-t_0)^2/T^2}$, where $V(t)$ is the electric field of an incident wave (V/m), t is time, t_0 is time delay, and T is the pulse width. The Gaussian pulse is used for the modeling because it contains multi-frequency information which can simulate wideband radar measurement, compared to a single frequency signal. The modeling scheme allows to select any frequency bandwidth of interests by changing the pulse width T as shown in FIG. 1. In this study, the incident Gaussian pulse is chosen to have a half power bandwidth of 5 GHz in frequency domain as shown in FIG. 2. The Gaussian pulse in time domain with the time delay t_0 = 0.2 ns[1] is shown in FIG. 1 with an

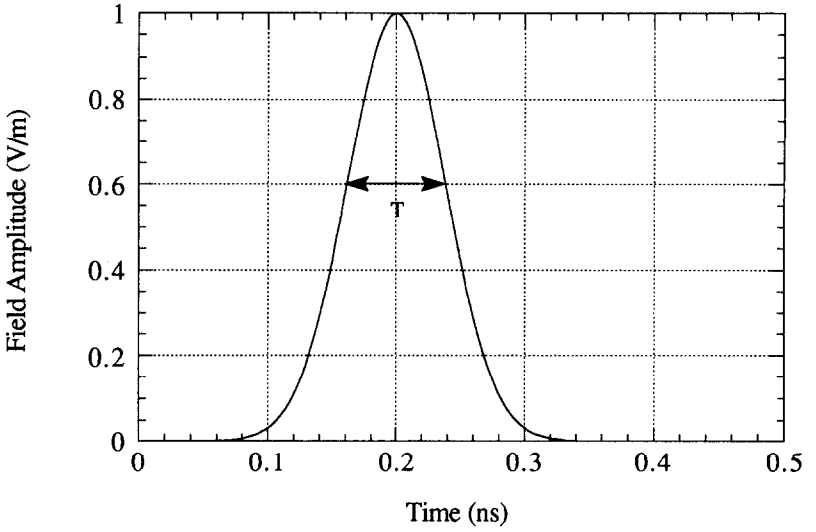

FIG. 1
The incident wave of a Gaussian pulse centered at the time delay of 0.2 ns with an amplitude of 1 V/m. The pulse width (T) is 0.0762 ns.

[1] nanosecond = 1×10^{-9} second

amplitude of 1 V/m as used in the modeling. The pulse width (T) of the incident wave is 0.0762 ns in time. The computational domain is shown in FIG. 3 and discretized by 800 by 1400 square grids. To achieve accurate results, the grid sizes are taken to be less than a fraction of (~ 1/10) of the smallest wavelength in any medium within the domain. Thus, 1.524 mm is used as a single grid size, which corresponds to a fraction of the wavelength at 5 GHz inside concrete specimens. Based on the grid size, the physical size of the computational domain is to be 1.2192 m x 2.1336 m. The detector which collects the reflected signal from the target is located at point A in FIG. 3. The physical distance between the detector and the outer boundary of the concrete cylinder is 0.9754 m. This puts the detector in the far field, based on the far field criterion (9), which gives 0.7742 m from the outer edge of the target. The incident field is a transverse electric, where the electric field is in z-direction in FIG. 3.

Laboratory Size Concrete Specimens

Three different types of laboratory size concrete specimens are used as targets for the modeling of wave scattering (FIG. 4). To examine the effects of different shape and size of the specimens, 152.4 mm diameter concrete cylinders (FIG. 4a), 152.4 mm x 152.4 mm concrete squares (FIG. 4b), and 609.6 mm x 152.4 mm concrete rectangles (FIG. 4c) are used. For each group of the specimens, three cases are considered involving no inclusion, an inclusion of a 25.4 mm diameter #8 steel reinforcing bar (rebar) located at the center, and a void of 25.4 mm diameter at the specimen center. The dimensions and configurations of these specimens are chosen so that they represent an initial and relatively simple set of laboratory size concrete targets and provide a basis for further study on more complex concrete targets. With the two-dimensional modeling, the third dimension of the specimen normal to the cross-section is assumed to be infinite.

The concrete specimens are characterized by their electromagnetic properties in the modeling. The electromagnetic properties of concrete used for the modeling are 4.8 for the dielectric constant and 0.15 mhos/m for the conductivity. These values represent measured electromagnetic properties at 5 GHz for normal strength concrete exposed to normal ambient temperature and humidity with uniaxial compressive strength of 21 MPa at 28 days and moisture content of 6.7% by weight (10). The specimens for the electromagnetic property measurements were cast with water/cement/sand mix ratio of 1:2:4 (by weight) with no coarse aggregates. A

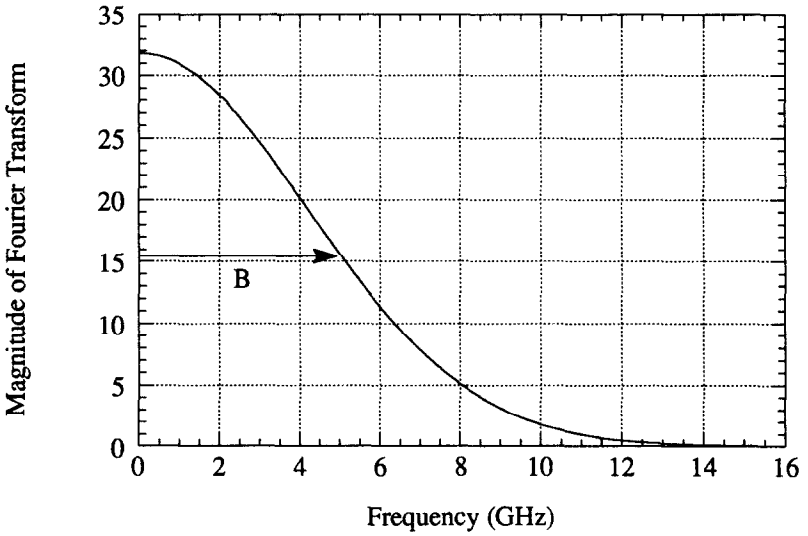

FIG. 2
The incident wave in frequency domain with a half power bandwidth of 5 GHz

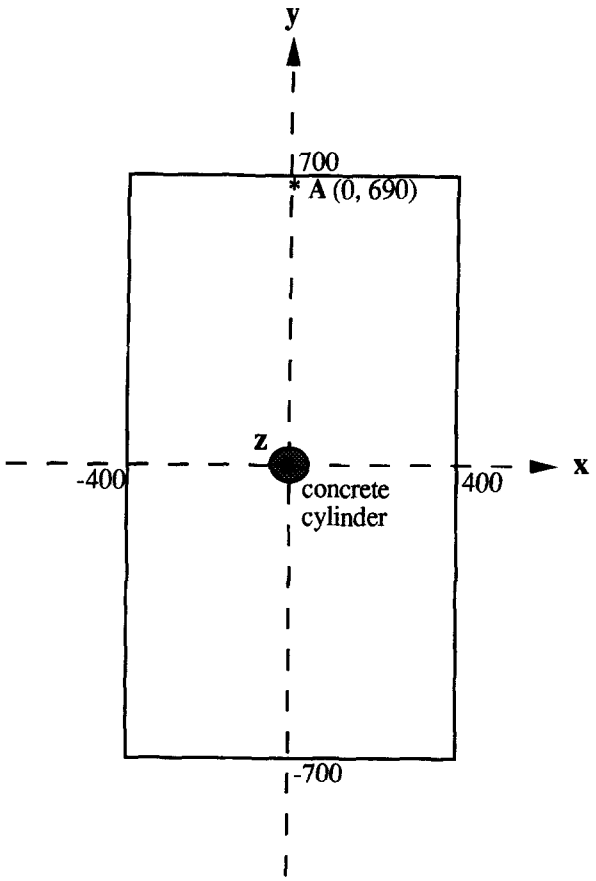

FIG. 3
A computational domain for the 2-D FD-TD modeling. The domain is discretized by 800 x 1400 square grids, where each grid size is 1.524 mm x 1.524 mm. A concrete specimen is located at the center of the computational domain. A cylindrical concrete specimen is shown as an example. Z direction is pointing out of the figure.

Portland cement of Type I was used. An open-ended coaxial probe method was used to measure the real and imaginary parts of the complex permittivity of the hardened concrete. The conductivity was deduced from the imaginary part of the measured values. The penetration depth (5) of concrete is 77.4 mm at 5 GHz.

The electromagnetic properties determine how concrete interacts with electric and magnetic fields of an incoming wave. One of the important aspects of the electromagnetic properties of concrete is that they vary with frequency and other physical conditions of concrete such as moisture content and density. In this modeling, a single set of constitutive parameters, dielectric constant and conductivity, is used because the dielectric constant does not vary with frequency over the frequency range up to 5 GHz and the variation of the conductivity is small enough that the single value of conductivity at 5 GHz can represent the property of concrete up to 5 GHz. Fixed values of the electromagnetic properties of concrete can be used for the modeling if these values are constant over the interested frequency range or the variation is negligible especially over a narrow bandwidth as the case presented in this paper. The changing electromagnetic properties of concrete can be also incorporated in the FD-TD modeling (11, 12).

(a) Cylindrical specimens with a 152.4 mm diameter

(b) Square specimens with dimensions of 152.4 mm x 152.4 mm

(c) Rectangular specimens with dimensions of 609.6 mm x 152.4 mm

FIG. 4
Laboratory size concrete specimens used for the modeling. Each group of specimens have either no inclusion, a 25.4 mm diameter rebar at the center, or a 25.4 mm diameter void at the center.

Simulation of Wave Propagation and Scattering

Results of the two-dimensional FD-TD simulation for the model of a 154.2 mm diameter concrete cylinder with a 25.4 mm diameter rebar at the center are shown in FIG. 5. The total electric field is shown at four instances of time. The magnitude of the electric field is represented by the intensity of the dark strip. The rebar is modeled as a perfect electric conductor.

In FIG. 5, the Gaussian pulse plane wave is directed from top to bottom in the picture. As the wave hits the front surface of the concrete cylinder, a part of the wave is reflected toward the direction where the wave came from and the remaining part of the wave is transmitted into the concrete continuing to propagate through the concrete cylinder. The slow-down of the wave inside concrete is clearly seen in FIG. 5b. The speed of the wave inside concrete is decreased by the dielectric constant, ε_r of 4.8 in this modeling, as $1/\sqrt{\varepsilon_r}$. As the wave passes through the rebar in FIG. 5c, another reflection occurs. In FIG. 5d, the last reflection occurs from the back surface of the cylinder as the wave completely moves away from the cylinder.

It should be noted that major reflections are coming from the boundaries where the material property discontinuity occurs (air/concrete, concrete/metal, or concrete/air). The significance of performing modeling of wave scattering as in this paper is to study detectability of such reflections from the boundaries for various types of concrete specimens. High order reflections inside the target and multiple reflections are taken into consideration by the modeling. In the following, one-dimensional images obtained as results of the simulation are provided.

1-D Images of Concrete Specimens Obtained From Modeling

One-dimensional images of three groups of the specimens are shown in FIG. 6, 7, and 8.

The images were obtained by capturing the reflected electric field at point A in FIG. 3. The received electric field is plotted as a function of time. The results of the cylindrical specimens are discussed first and compared to the square and rectangular specimens.

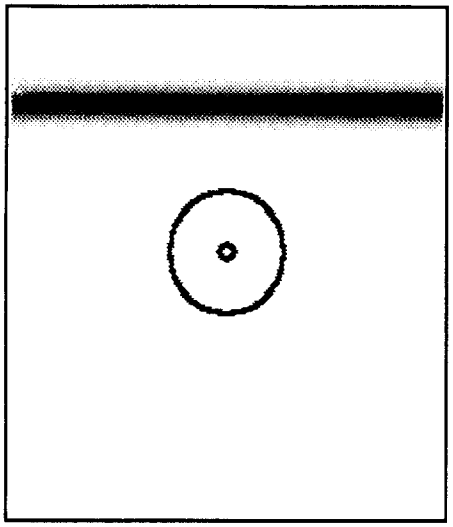

(a) A plane wave is directed from the top.

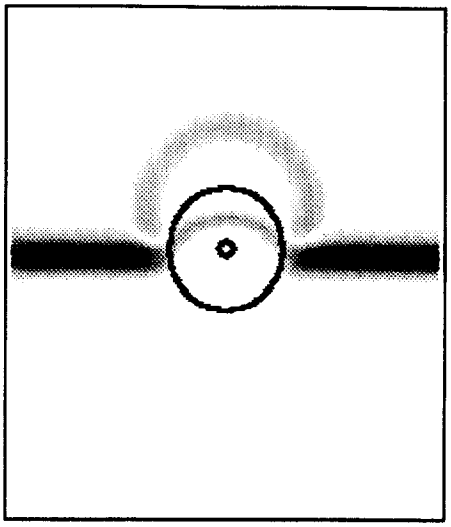

(b) The wave hits the concrete cylinder.

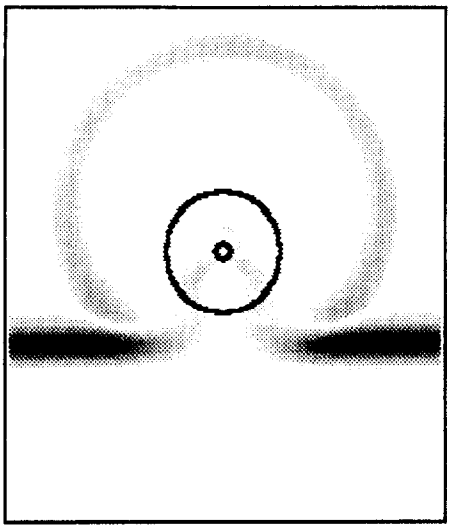

(c) The wave propagates through the cylinder.

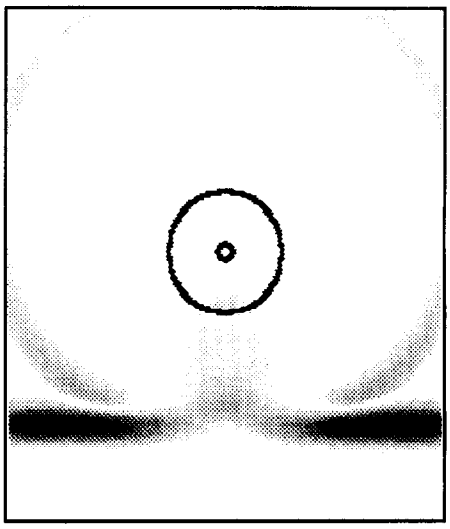

(d) The wave leaves the cylinder.

FIG. 5
Two-dimensional FD-TD simulation of wave scattering by a 152.4 mm diameter concrete cylinder with a 25.4 mm diameter steel reinforcing bar at the center. The electric field is polarized perpendicular to the picture. The dielectric constant of concrete is 4.8 and conductivity is 0.15 mhos/m. The time width of the incident Gaussian pulse is 0.0762 ns.

In FIG. 6a, for the case of a plain concrete cylinder with no inclusion, the region around the peaks B and C correspond to the front and back surfaces of the cylinder, respectively. These peaks are clearly identified by tracing the reflections from the computer run as shown in FIG. 5. The negative sign of B comes from the reflection coefficient at the air/concrete boundary, which is the front surface of the concrete cylinder. The positive sign of C comes from the reflection coefficient at the concrete/air boundary, which is the back surface of the cylinder. These examinations of the sign of reflection coefficients confirm the identification of the peaks. The diameter of the cylinder can be calculated by taking the difference between the peaks and multiplied by the speed of wave inside concrete, which is reduced by the permittivity of concrete. Then, the total distance is divided by 2 for one way distance as:

$$\text{distance} = \text{velocity x time}$$

$$= \frac{c}{\sqrt{\varepsilon_r}} \text{ x time difference / 2}$$

where c is speed of wave in air = $3x10^8 m/s$ and ε_r is the permittivity of concrete. The calculated distances are summarized in Table 1.

In FIG. 6b, for the case of a concrete cylinder with a 25.4 mm diameter rebar at the center, the front and back surfaces of the cylinder are captured as peaks B and C. The third peak D represents the rebar. This image is obtained from the simulation shown in FIG. 5. The locations of the peaks B and C do not change due to the rebar when they are compared to the ones in FIG. 6a. Instead, the magnitude of the peak C decreased compared to FIG. 6a because of high scattering due to the rebar. The sign of D in the negative direction confirms that it is a reflection from an electric conductor. This interpretation can be made by examining the transmission and reflection coefficients of the two different media.

In FIG. 6c, for the case of a concrete cylinder with a 25.4 mm diameter void at the center, the peak E represents the presence of the void. Again, the locations of the peaks B and C do not change due to the void when they are compared to the ones in FIG. 6a. Unlike the case with a rebar, the magnitude of peak C does not decrease due to the void. The peak E is positive indicating the wave is reflected at the concrete/air boundary, which is the front surface of the void. As the wave gets back into the concrete after passing the void, the sign of the electric field changes to negative as shown in peak F.

The one-dimensional images obtained from the cylindrical specimens clearly capture the existence of the target and its inclusion of the rebar or void at a distance of 0.9754 m. Results of the modeling for square and rectangular specimens are shown in FIG. 7 and 8. The larger magnitude of reflections from the front surfaces are noticed with the square and the rectangular specimens compared to those of the cylindrical specimens. This is due to the larger contact area of the surface exposed to the incoming electromagnetic waves. Edge effects are shown with the square and rectangular specimens, which are not observed with the cylindrical specimens. The calculated distances between the front and the back surfaces and the locations of the inclusions for the three different types of the specimens are summarized in Table 1.

Discussion

The results of the FD-TD modeling scheme demonstrate the capability of the method in detecting the front and back surfaces of the specimens as well as the inclusions embedded inside. Identification of these reflections are possible by visually following the reflections shown on the computer screen as a function of time, by examining the sign of the reflection coefficients, and by comparing the calculated distances between the peaks to the actual dimensions of the target.

The cylindrical targets produce smoother reflected signals compared to the square and rectangular shaped targets. For all three types of specimens, the location of the first reflection from

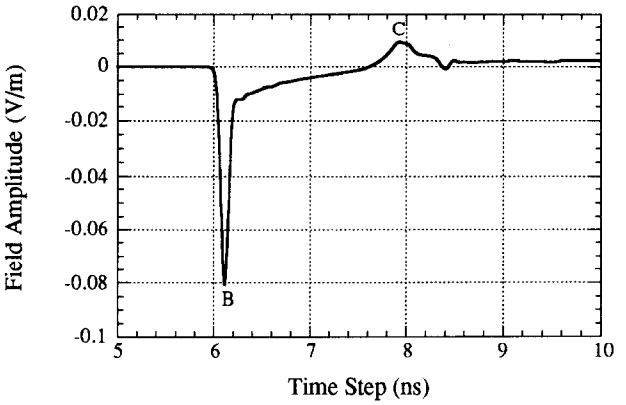

(a) Cylindrical specimen with no inclusion

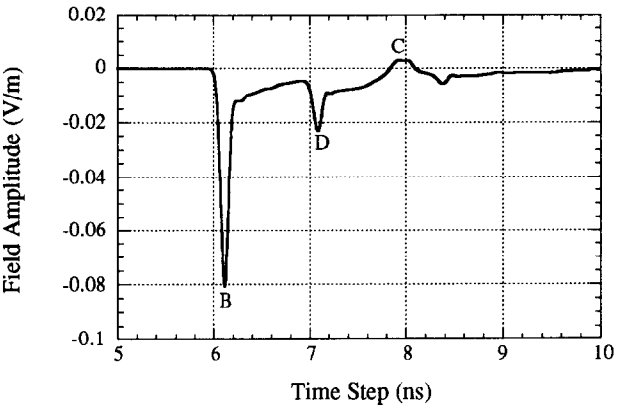

(b) Cylindrical specimen with a 25.4 mm diameter rebar at the center

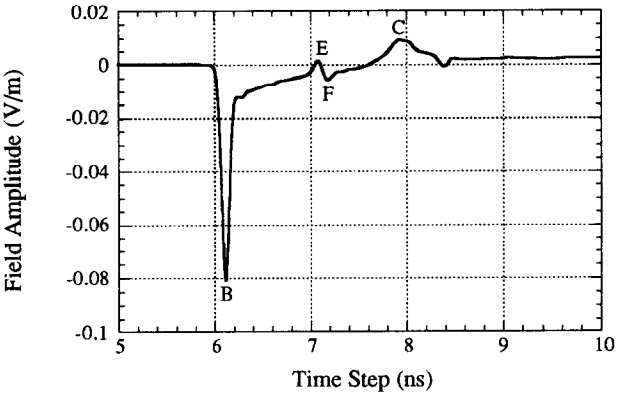

(c) Cylindrical specimen with a 25.4 mm diameter void at the center

FIG. 6 One-dimensional images of 152.4 mm diameter cylindrical concrete specimens

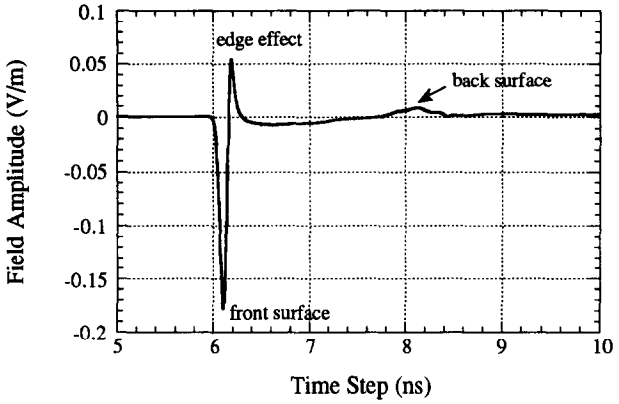

(a) Square specimen with no inclusion

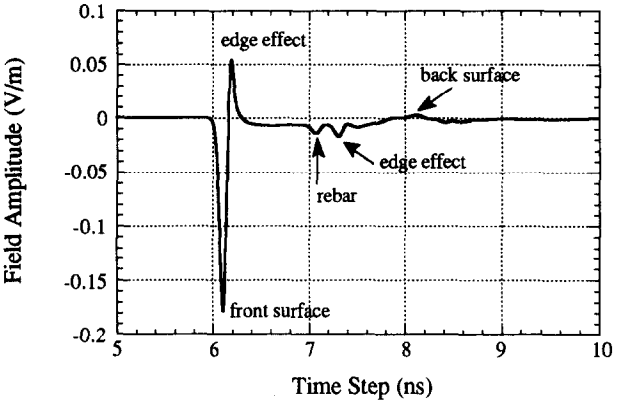

(b) Square specimen with a 25.4 mm diameter rebar at the center

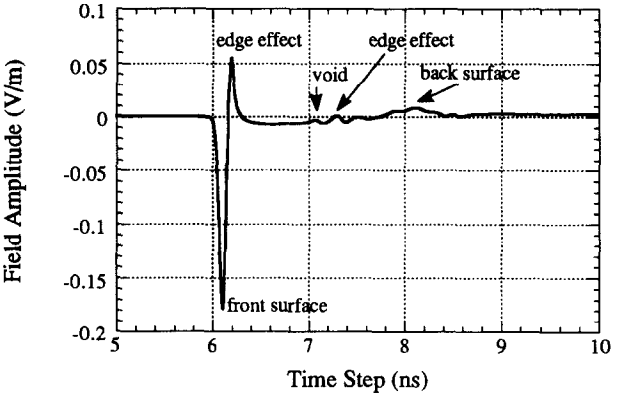

(c) Square specimen with a 25.4 mm diameter void at the center

FIG. 7 One-dimensional images of 152.4 mm x 152.4 mm square concrete specimens

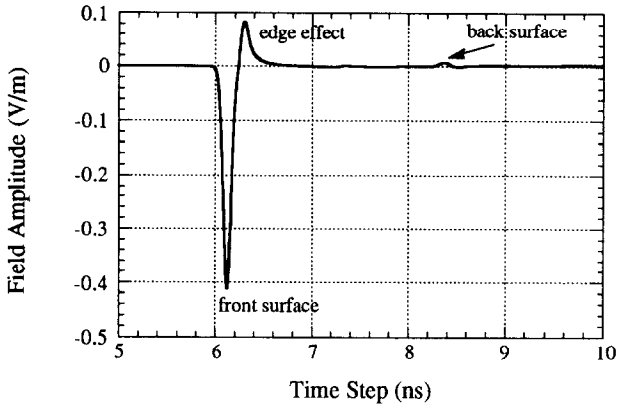

(a) Rectangular specimen with no inclusion

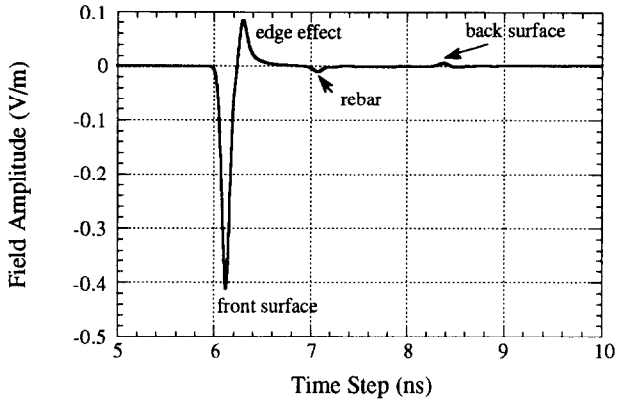

(b) Rectangular specimen with a 25.4 mm diameter rebar at the center

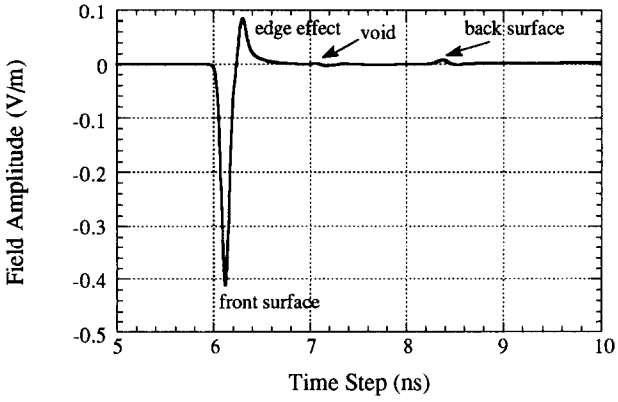

(c) Rectangular specimen with a 25.4 mm diameter void at the center

FIG. 8 One-dimensional images of 609.6 mm x 152.4 mm rectangular concrete specimens

TABLE 1
Calculated distances between material boundaries obtained from the numerical modeling

Concrete Specimens	Cylinders (152.4 mm diameter)	Squares (152.4 mm x 152.4 mm)	Rectangles (609.6 mm x 152.4 mm)
a) Front to back surface distance actual: 152.4 mm	124.32 mm	137.29 mm	155.66 mm
b) Front surface to rebar distance actual: 63.5 mm	64.86 mm	65.94 mm	65.94 mm
c) Front surface to void distance actual: 63.5 mm	64.86 mm	65.94 mm	65.94 mm

the front surface is the same indicating that there is no shape or dimension effect on the front surface reflection. However, for the back surface reflection, cylindrical specimens produce earlier return than the squares and the rectangles due to creeping wave mechanism, which is a phenomenon generally associated with smooth bodies. Both the square and the rectangular specimens show edge effects. The edge effect is more severe with the square specimens when there is an inclusion. The wave interacting with edges interrupts the signal from the inclusions as seen in FIG. 7b and 7c. The rectangular specimens give good results in picking up the dimensions of the whole target and the location of the inclusions. The locations of inclusions for rectangular specimens are clearly seen in the larger scale plots for clarity.

The source of error for the FD-TD modeling comes from the fact that the target is discretized and modeled by square grids. Curved edge of cylinders are approximated by squares. The computational domain has open boundary condition simulating open air measurement. Absorbing boundary condition applied in the modeling can have a certain error, even though it should absorb any reflection passing through the outer boundary of the domain.

Another aspect of this modeling is that it incorporates the measured electromagnetic properties of concrete as input data. The physical condition of concrete and the frequency of incoming wave determine the electromagnetic properties of concrete. If the frequency dependency of the property is small or the incident wave has narrow frequency bandwidth, constant values of the properties may be used as in this modeling. Incorporation of changing electromagnetic properties is possible but may not be absolutely necessary, if the variation is negligible.

Conclusion

Simulation of electromagnetic wave propagation and scattering through and by concrete specimens is performed using the finite difference-time domain (FD-TD) method. A Gaussian pulse plane wave centered at the direct current with a half power bandwidth of 5 GHz and an amplitude of 1 V/m is directed to the three types of laboratory size concrete specimens with or without an inclusion. The propagation of the electromagnetic fields in a dielectric medium of concrete is visualized and one-dimensional images are obtained as results. The size of the concrete specimens and locations of the inclusions are predicted through modeling. The findings also suggest that the shape and size of the outer geometry of targets affect the detectability of targets and inclusions inside. The numerical modeling scheme of the FD-TD method is shown to be an effective means to predict electromagnetic phenomena associated with concrete targets for nondestructive testing purposes. Future work will involve laboratory experimentation for comparison with the numerical modeling results.

Acknowledgments

The authors wish to thank Dr. Tony C. Liu and Mr. Mitch Alexander of U.S. Army Corps of Engineers for the financial support provided through Contract #DACW39-92-K-0029. Computational facilities were provided by the Center for Electromagnetic Theory and Application in the Department of Electrical Engineering and Computer Science at MIT.

References

1. Clemeña, G.G., "Short-Pulse Radar Methods," *CRC Handbook on Nondestructive Testing of Concrete*, Editors, V.M. Malhotra and N.J. Carino, CRC Press, pp. 253-274, 1991.

2. Holt, F.B. and Eales, J.W., "Nondestructive Evaluation of Pavements," *Concrete International*, June, pp. 41-45, 1987.

3. Chung, T., Carter, C.R., Masliwec, T., and Manning, D.G., "Impulse Radar Evaluation of Asphalt-Covered Bridge Decks," *IEEE Transactions on Aerospace and Electronic Systems*, Vol. 28, No. 1, pp. 125-137, January 1992.

4. Büyüköztürk, O., Rhim, H.C., and Blejer, D.J., "Application of Radar Imaging Techniques to Concrete," *Proceedings of a Conference on Digital Image Processing: Techniques and Applications in Civil Engineering*, Editors, J.D. Frost and J.R. Wright, Sponsored by the Engineering Foundation and the National Science Foundation, Published by the American Society of Civil Engineers, Kona, Hawaii, pp. 142-149, February 28 - March 5, 1993.

5. Shen, L.C. and Kong, J.A., *Applied Electromagnetism*, 2nd Ed., PWS Engineering, Boston, Massachusetts, 1987.

6. Taflove, A., "Review of the Formulation and Applications of the Finite-Difference Time-Domain Method for Numerical Modeling of Electromagnetic Wave Interactions with Arbitrary Structures," *Wave Motion*, Vol. 10, pp. 547-582, 1988.

7. Li, K., Tassoudji, M.A., Shin, R.T., and Kong, J.A., "Simulation of Electromagnetic Radiation and Scattering Using a Finite Difference-Time Domain Technique," *Computer Applications in Engineering Education*, Vol. 1(1), pp. 45-63, September/October 1992.

8. Engquist, B. and Majda, A., "Absorbing Boundary Conditions for the Numerical Simulation of Waves," *Mathematics of Computation*, Vol. 31, No. 139, pp. 629-651, July 1977.

9. Knott, E.F., Shaeffer, J.F., and Tuley, M.T., *Radar Cross Section*, Artech House Inc., Dedham, Massachusetts, 1985.

10. Büyüköztürk, O. and Rhim, H.C., "Electromagnetic Properties of Concrete for Nondestructive Testing," *Proceedings of the International Conference on Nondestructive Testing of Concrete in the Infrastructure*, Society for Experimental Mechanics, Dearborn, Michigan, pp. 83-92, June 9 -11, 1993.

11. Lee, C.F., Shin, R.T., and Kong J.A., "Finite Difference Method for Electromagnetic Scattering Problems," *PIER 4 Progress In Electromagnetics Research*, Editor, J.A. Kong, Elsevier Science Publishing Co., New York, New York, pp. 373-442, 1991.

12. Joseph, R.M., Hagness, S.C., and Taflove, A., "Direct Time Integration of Maxwell's Equations in Linear Dispersive Media with Absorption for Scattering and Propagation of Femtosecond Electromagnetic Pulses," *Optics Letters*, Vol. 16, No. 18, pp. 1412-1414, September 15, 1991.